

PCCP

Accepted Manuscript



This is an *Accepted Manuscript*, which has been through the Royal Society of Chemistry peer review process and has been accepted for publication.

Accepted Manuscripts are published online shortly after acceptance, before technical editing, formatting and proof reading. Using this free service, authors can make their results available to the community, in citable form, before we publish the edited article. We will replace this *Accepted Manuscript* with the edited and formatted *Advance Article* as soon as it is available.

You can find more information about *Accepted Manuscripts* in the [Information for Authors](#).

Please note that technical editing may introduce minor changes to the text and/or graphics, which may alter content. The journal's standard [Terms & Conditions](#) and the [Ethical guidelines](#) still apply. In no event shall the Royal Society of Chemistry be held responsible for any errors or omissions in this *Accepted Manuscript* or any consequences arising from the use of any information it contains.

Electron Spin-Polarization and Spin Lattices in Boron- and Nitrogen-Doped Organic Framework COF-5

Xiaobiao Liu, Jie Tan, Aizhu Wang, Xiaoming Zhang, Mingwen Zhao*

School of Physics and State Key Laboratory of Crystal Materials, Shandong University, Jinan,

Shandong, 250100, China

Abstract

Covalent organic frameworks (COFs) hold great promises in many applications, such as sieves, catalytic supports, gas storage, etc., due to the unique structures and electronic properties. However, most of these metal-free COFs are nonmagnetic and can not be used directly in spintronics. Here, based on first-principles calculations, we predict that substitutional doping of COF-5 with nitrogen and boron atoms can modify the electronic structures, inducing stable electron spin-polarization in the framework. The preferability of the different doping sites is checked. The electronic structures of the doped COF-5 are dependent on the doping sites and doping atoms, which offers more degree of freedom to tune the electronic properties. Kagome lattices of $S = 1/2$ spins can be achieved in the COF-5, suggesting a promising candidate for spin-liquid materials.

*Electronic mail: zmw@sdu.edu.cn

Introduction

Covalent organic frameworks (COFs) are new class of crystals composed entirely of light chemical elements such as C, N, H, O, and B. Due to the strong covalent bonds in the frameworks, COFs exhibit good thermal stability. In addition to their low gravimetric density and large surface areas, COFs feature with versatile electronic behaviors, making them ideal candidates for sieves, catalytic supports, gas storage especially in H₂ storage, and semiconducting and optoelectronic applications [1-7]. Through solvothermal condensation of 1,4-phenylenebis(boronic acid)(PBBA) and 2,3,6,7,10,11-hexahydroxytriphenylene(HHTP), Côté *et al.* synthesized a COF material referred to as COF-5 [8]. COF-5 membrane can also be fabricated on a commonly used porous α -Al₂O₃ support by using a microwave irradiation method [9]. In a recent work of Colson and his co-workers, COF-5 monolayer was firstly achieved [10]. Inspired by these experimental progresses, considerable efforts have been devoted to this layered porous structure. Recently, the electronic and optical properties of COFs are drawing increasing attention, due to applications in nanoscaled devices. For example, a theoretical work shows that COF-5 exhibits a type-II heterojunction alignment with significant valence and conduction band offsets, suggesting an effective spatial carrier separation of electrons and holes [2]. The work of Lukose *et al.* indicates that the electronic density of states of a COF monolayer is very similar to those of the multilayers [11]. The band gaps of COFs can be tuned by changing the organic chain-links in the framework, but are less affected by the substrates [12]. However, the COF materials considered in these works are spin-unpolarized, and thus can not be used directly in spintronics devices. Therefore, inducing stable electron spin-polarization in COFs becomes an interesting issue, which will broaden the applications of these materials.

Here, based on first-principles calculations, we predict that COF-5 monolayer can be tuned to a spin-polarized metallic or semiconducting material by substitutional B or N doping. The electronic structure modification of the B- and N-doped COF-5 materials is dependent on many factors, such as doping sites, dopant species, and doping concentration, offering more degree of freedom to tune the electronic properties. More interestingly, a kagome lattice of $S = 1/2$ spins can be achieved in the COF-5, suggesting a promising candidate for spin-liquid materials. Spin-liquid states and their host materials have been drawing considerable attentions for many years [13-16]. However, nearly all of these spin-liquid materials contain transition metals. The candidate we proposed here is free from metal atoms, and thus may bring about new physical phenomena.

Computational details

Our first-principles calculations were performed using the Vienna ab initio simulation package known as VASP [17, 18] code, implementing density functional theory (DFT). The projector augmented wave method (PAW) [19] was used to describe the electronic-ion-core interaction. The energy cutoff of the plane waves was set to 520 eV with the energy precision of 10^{-5} eV. The electron exchange-correlation function was treated using a generalized gradient approximation (GGA) in the form proposed by Perdew, Burke, and Ernzerhof (PBE) [20]. In order to save computational resources, only Γ point was used for the Brillouin zone (BZ) integration for structure optimization, whereas a $3 \times 3 \times 1$ k-point grid according to the Monkhorst-Pack scheme [21] was used for electronic structure calculations. We have verified that single Γ point is enough for the structure optimization of such large supercells. The supercell was repeated periodically along the x- and y-directions, while a vacuum region up to 15 Å was applied along the z-direction to exclude the interaction between adjacent images. Both atomic positions and lattice vectors were fully optimized using the conjugate

gradient (CG) algorithm until the maximum atomic forces were less than 0.01 eV/Å.

Results and discussion

The primitive cell of COF-5 consists of two types of units: PBBA and HHTP. PBBA units are linked together by HHTPs, forming a honeycomb lattice of PBBA, as shown in Fig. 1. Each supercell has 54 carbon, 12 oxygen, 6 boron and 24 hydrogen atoms. The optimized lattice constant (the length of base vectors) is 30.2 Å, in good agreement with the experimental data (29.9 Å) [10] and those of the previous theoretical work [2]. The COF-5 monolayer has a perfect planar configuration without any buckling. The bond lengths and bond angles are listed in Table 1. It is interesting to see that the PBBA units form a typical kagome lattice that consists of corner-sharing triangles, as indicated by the blue dotted lines in Fig. 1(d). Kagome lattices display novel physical properties connected with geometrically frustrated magnetism. Of particular interest is that antiferromagnetic coupling spins 1/2 on a Kagome lattice support a spin liquid ground state [22]. Different arrangements of the PBBA and HHTP units in the COF-5 framework will affect the electronic properties.

The electronic band structures of the COF-5 monolayer are plotted in Fig. 2(a). Clearly, COF-5 is a semiconductor with a band gap of 2.5 eV. Due to the failure of PBE functional in reproducing the band gap of semiconducting materials, the band gap is underestimated. Using a more accurate Heyd-Scuseria-Ernzerhof (HSE) screened Coulomb hybrid density functional [23], the band gap of COF-5 monolayer is increased to 3.3 eV from the present calculations. The valence band maximum (VBM) and conduction band minimum (CBM) are contributed by different blocks of the framework. The VBM states arise mainly from the HHTP blocks, while the CBM states are contributed by the PBBA blocks, as shown in Fig.2(b) and Fig.2(c). These results are consistent with those of previous

work [2]. The separation of CBM and VBM is beneficial for the applications of photovoltaic devices.

It is interesting to see that the three conduction bands (red lines) nearest to the Fermi level exhibit clear features of the kagome bands, i.e., one flat band above two Dirac bands, as revealed in many kagome lattices [24-26]. These three bands are contributed mainly by the PBBA blocks as indicated by the Kohn-Sham wavefunctions shown in Fig. 2(b). The PBBA blocks form a kagome lattice in the framework of COF-5. The appearance of the kagome bands is therefore reasonable. For the four valence bands (purple lines) close to the Fermi level, the features of topical ruby bands are very obvious, i.e., two Dirac bands sandwiched by two flat bands [27, 28]. This is related to the honeycomb arrangement of the HHTP blocks, which contribute largely to the four valence bands. Both kagome model and ruby model have been proposed as candidates to achieve quantum spin Hall effects (QSHE) and fractional quantum hall effects (FQHE) [25, 28]. The two models coexist in the COF-5 framework. Of course, we should notice that pristine COF-5 is a trivial semiconductor. The Fermi level should be moved to the kagome bands or ruby bands region, for example by applying gate voltage or electron/hole doping, to achieve QSHE and FQHE [32]. This is beyond the scope of the present work.

We turn to the possible carbon sites for doping COF-5 with B and N atoms. Due to the symmetry (P6/mmm) of COF-5, there are five non-equivalent carbon atoms labeled as C_i ($i=1-5$) as shown in Fig. 1(c). The preference of N and B atoms at these carbon sites can be deduced from the energies of the relevant doped structures. Hereafter, we denote a COF-5 with a C_i being replaced by one N (or B) atom in a unit cell as COF5-N_{*i*}(or COF5-B_{*i*}). The energies corresponding to different sites of the N- and B-doped COF-5 monolayers are plotted in Fig. 3. From this figure, we can see

clearly that N prefers to replace the C₂ atom at PBBA, while B favors the C₃ site at HHTP. This trend can be easily understood in terms of the electron configurations of B and N and the different contributions of PBBA and HHTP to the electronic structures. When one N (or B) atom replaces one carbon atom of the COF-5, an extra electron (or a hole) is introduced into the system. The extra electron (or hole) prefers to occupy conduction (or valence) bands, which are contributed by the PBBA (or HHTP) blocks. N atom whose electronegativity is larger than that of both C and N atoms prefers to bond to one B and two C atoms. B atom has smaller electronegativity than C atom and thus prefers to bond to the O atom of HHTP. The energy of the second lowest doping configuration relative to the lowest one is about 0.42 eV (for N doping) and 0.85 eV (for B doping). Such large energy differences are advantageous for oriented substitutional doping. Therefore, in the following parts, we focus on the two doping configurations that are energetically most favorable.

The structural parameters and the variation of bond lengths of COF5-N₂ and COF5-B₃ are listed in Table 1. We can see that the structural distortion due to B substitution is more significant than that of N doping. Structural distortion mainly takes place in the region near the doping sites. The B-N bond length in COF5-N₂ is about 1.438 Å, shorter than that of the B-C bond by about 6.8%. The length of the bond between the dopant atom B and C is 1.500 Å, longer than that of the C-C bond by about 9.3%. The changes of other bonds are smaller than 1.8%. In addition, the structure of HHTP building block is negligibly affected by doping PBBA building block, and vice versa. This phenomenon implies that the properties of those two building blocks can be tuned separately without influence each other. This feature is quite promising for design of functionalized molecular devices.

The plausibility of doping COF-5 framework with N and B atoms can also be hinted by the substitution energy (E_{sub}) defined as:

$$E_{sub} = E_{doped} - E_{undoped} - n \times (\mu_{B/N} - \mu_C)$$

E_{doped} and $E_{undoped}$ are the total energies of doped and undoped COF-5 frameworks. $\mu_{B/N}$ and μ_C are the chemical potentials of B (or N) and C atoms, which are calculated from α -B₁₂ crystal (or N₂ molecule) and graphene. n is the number of doping atoms. The calculated substitution energies are 0.16 eV for COF-N₂ and 0.04 eV for COF-B₃, respectively. The low E_{sub} values suggest the high possibility of the doped configurations. From the experimental points of view, B- and N-doped carbon materials, such as graphene and nanotube derivatives, have been achieved successfully using thermal treatment with boron compounds, N₂ microwave plasma technique, or reduction-oxidation methods [30-35]. These strategies may be useful for the realization of B- and N-doped COF-5 frameworks.

The spin-resolved electronic density of states (DOS) of COF5-N₂ and COF5-B₃ are plotted in Fig. 4(a). The data of pristine COF-5 is also presented for propose of comparison. It is clear that both B and N doping induce localized electronic states within the band gap of pristine COF-5. These states are close to the conduction band region and valence band region, respectively, in good agreement with the above analysis. Moreover, they are spin-polarized, leading to a magnetic moment of 1 μ_B per unit cell for both cases. The spin-polarized states are the ground states and lower in energy than the spin-unpolarized states by 102 meV (for COF5-N₂) and 80 meV (for COF5-B₃), implying that the magnetic moments are stable even at room temperature. The spin splitting in COF5-N₂ is more significant than that in COF5-B₃. The offset of two spin branches is about 1.6 eV for COF5-N₂, whereas the spin splitting in COF5-B₃ takes place only near the Fermi level with an offset of 0.3 eV. The spatial distribution of the spin-polarized electronic density calculated from the difference between the charge densities of the two spin branches, $\Delta\rho = \rho_{\uparrow} - \rho_{\downarrow}$, is shown in Fig. 4(b) and (c). From this figure, we can see that the spin-polarized electrons reside mainly at the building blocks

where the doping atoms lie in. For instance, the spin polarized electronic density of COF5-N₂ distributes in the PBBA block, while that induced by the doped B atom spreads to the center of HHTP rings, instead of locating at the region near the doping sites. In addition, the impurities break the symmetry of the original system, leading to a decrease of degeneracy and the band spitting.

Finally, we consider the COF-5 monolayer with a higher doping concentration, i.e., three dopant atoms per unit cell, corresponding to a doping concentration of 3.1 at%. Two doping configurations of COF5-3N₂ and COF5-3B₃ shown in Fig. 5 are considered. The corresponding electronic band structures and density of states are plotted in Fig. 6. Obviously, COF5-3N₂ is a spin-polarized semiconductor with a band gap of 0.3 eV, which is much narrower than that of pristine COF-5. Although, PBE functional always underestimates the band gap of semiconductors, it still gives the general trend of band gaps among different architectures. N doping makes the three kagome bands fully spin-polarized, leading to local magnetic moments of 3 μ_B per unit cell. A small band gap opens up between the two Dirac bands at K points in BZ, due to the doping-induced symmetry breakage. The band gaps are 13 meV and 18 meV for spin-up and spin-down branches. For COF5-3B₃, both band structures and DOS imply that it is a half metal, i.e., one spin channel is metallic with bands across the Fermi level, while another spin channel is semiconducting with a band gap of 0.6 eV. The magnetic moments of the COF5-3B₃ are 1 μ_B per unit cell. This is related to the interactions between the three dopant atoms (B) in the same HHTP block. These features are very promising for building spintronics devices.

It is interesting to see that the spatial distribution of the spin-polarized electronic density is highly localized. The spin-polarized electrons of the COF5-3N₂ reside at the PBBA blocks of the framework, which are well separated by the HHTP blocks. Each PBBA block contains a local

magnetic moment of $1 \mu_B$, corresponding to a spin of $S = 1/2$. Considering the configuration of PBBA blocks, a kagome lattice of spins ($S = 1/2$) can be achieved in the COF5-3N₂, as shown in Fig. 5(a). Kagome lattice of spins has been proposed as a model system to realize spin-liquid states [22]. So far, most of the candidate materials contain transition metals. Our work suggests that spin-liquid states may be realized in the metal-free framework. The spins in the COF5-3N₂ is quite stable. The spin-polarized state is lower in energy than the spin-unpolarized one by 104 meV per PBBA block, sufficiently higher than the energy of thermal motion at room temperature, 26 meV. The wavefunctions of the PBBA blocks are separated by HHTP blocks. The interactions between adjacent spins are thus expected to very weak. These features facilitate the realization of spin-liquid states in this material. Additionally, substrate is inevitable in real devices, which may destroy the spin states of the doped COF-5 frameworks. The robustness of the spins in the presence of substrate is therefore crucial. The effect of substrate can be minimized by using inert substrate materials with large band gap, such as hexagonal boron nitride [36-39], to avoid electronic state hybridization and charge transfer between COF-5 and substrate. However, due to computational limitation, the substrate effects can not be studied directly from first principles calculations at present.

Conclusions

From first-principles calculations, we demonstrate theoretically that the kagome bands and ruby bands coexist in the band structures of COF-5, which are contributed by the PBBA and HHTP building blocks, respectively. The electronic properties can be effectively modified by substitutional doping of COF-5 with boron or nitrogen atoms. N atom prefers to replace the C atom of the PBBA block, whereas B atom favors the substitution of the C atom of the HHTP block. Both N and B dopants can induce stable electron spin-polarization locating at the PBBA and HHTP blocks

separately in the metal-free COF-5. In contrast to the wide-band-gap features of pristine COF-5, COF-3B₃ is a half-metal, while COF-3N₂ is a spin-polarized semiconductor with a narrow band gap. A kagome lattice of spins ($S=1/2$) can be achieved in the metal-free COF-3N₂, which is quite promising for realizing spin-liquid states. Such abundant phenomena will broaden the applications of the COF-5 framework.

Acknowledgements

This work is supported by the National Basic Research Program of China (No. 2012CB932302), the National Natural Science Foundation of China (No. 91221101), the 111 project (No. B13209) and National Super Computing Centre in Jinan.

References

- 1 W. Shun, G. Jia, K. Jangbae, I. Hyotcherl and J. Donglin, *Angew. Chem.*, 2008, **120**, 8958-8962.
- 2 Y. Zhou, Z. Wang, P. Yang, X. Zu and F. Gao, *J. Mater. Chem.*, 2012, **22**, 16964-16970.
- 3 G.H. Fan, X. Li, J.Y. Liu and G.Z. He, *Comput.Theor. Chem.*, 2014, **1030**, 17-24.
- 4 K. T. Jackson, M. G. Rabbani, T. E. Reich and H. M. El-Kaderi, *Polym.Chem.*, 2011, **2**, 2775-2777.
- 5 Y. J. Choi, J. H. Choi, K. M. Choi and J. K. Kang, *J. Mater. Chem.* 2011, **21**, 1073-1078.
- 6 X. D. Li, J. H. Guo, H. Zhang, X. L. Cheng and X. Y. Liu, *RSC Adv.*, 2014, **4**, 24526-24532.
- 7 J. H. Guo, H. Zhang, Y. Tang and X. Cheng, *Phys. Chem. Chem. Phys.*, 2013, **15**, 2873-2881.
- 8 A. P. Cote, A. I. Benin, N. W. Ockwig, M. O'Keeffe, A. J. Matzger and O. M. Yaghi, *Science*, 2005, **310**, 1166-1170.
- 9 D. Hao, J. Zhang, H. Lu, W. Leng, R. Ge, X. Dai and Y. Gao, *Chem. Commun.*, 2014, **50**, 1462-1464.
- 10 J. W. Colson, A. R. Woll, A. Mukherjee, M. P. Levendorf, E. L. Spitler, V. B. Shields, M. G. Spencer, J. Park and W. R. Dichtel, *Science*, 2011, **332**, 228-231.
- 11 B. Lukose, A. Kuc, J. Frenzel and T. Heine, *Beilstein J. Nanotech.*, 2010, **1**, 60-70.
- 12 P. Zhu and V. Meunier, *J. Chem. Phys.*, 2012, **137**, 244703.
- 13 Y. Okamoto, M. Nohara, H. Aruga-Katori and H. Takagi, *Phys. Rev.Lett.*, 2007, **99**, 13207.
- 14 Y. Shimizu, K. Miyagawa, K. Kanoda, M. Maesato and G. Saito, *Phys. Rev. Lett.*, 2003, **91**, 107001.
- 15 L. Balents, *Nature*, 2010, **464**, 199-208.
- 16 J. Knolle, D. L. Kovrizhin, J. T. Chalker and R. Moessner, *Phys. Rev.Lett.*, 2014, **112**, 207203.

- 17 G. Kresse and J. Furthmüller, *Phys. Rev. B*, 1996, **54**, 11169.
- 18 G. Kresse and J. Hafner, *Phys. Rev. B*, 1998, **48**, 13115.
- 19 G. Kresse and D. Joubert, *Phys. Rev. B*, 1999, **59**, 1758.
- 20 J. P. Perdew, K. Burke and M. Ernzerhof, *Phys. Rev.Lett.*, 1996, **77**, 3865-3868.
- 21 H. J. Monkhorst and J. D. Pack, *Phys. Rev. B*, 1976, **13**, 5188-5192.
- 22 S. Yan, D. A. Huse and S. R. White, *Science*, 2011, **332**, 1173-1176.
- 23 J. Heyd, G. E. Scuseria and M. Ernzerhof, *J. Chem. Phys.*, 2006, **124**, 219906.
- 24 M. Zhao, A. Wang and X. Zhang, *Nanoscale*, 2013, **5**, 10404-10408.
- 25 E. Tang, J.W. Mei and X.G. Wen, *Phys. Rev. Lett.*, 2011, **106**, 236802.
- 26 Z. F. Wang, N. Su and F. Liu, *Nano Lett.*, 2013, **13**, 2842-2845.
- 27 T. Liu, C. Repellin, B. A. Bernevig and N. Regnault, *Phys. Rev. B*, 2013, **87**, 205136.
- 28 X. Hu, M. Kargarian and G. A. Fiete, *Phys. Rev. B*, 2011, **84**, 155116.
- 29 A. Wang, X. Zhang and M. Zhao, *Nanoscale*, 2014, DOI: 10.1039/C4NR02707H.
- 30 D. Cai, D. Li, S. Wang, X. Zhu, W. Yang, S. Zhang and H. Wang, *J. Alloy. Compd.*, 2013, **561**, 54-58.
- 31 J. Han, J. Y. Cheon, S. H. Joo and S. Park, *Solid State Sci.*, 2014, **33**, 1-5.
- 32 S. M. Jung, E. K. Lee, M. Choi, D. Shin, I. Y. Jeon, J. M. Seo, H. Y. Jeong, N. Park, J. H. Oh and J. B. Baek, *Angew. Chem.*, 2014, **53**, 2398-2401.
- 33 L. Niu, Z. Li, W. Hong, J. Sun, Z. Wang, L. Ma, J. Wang and S. Yang, *Electrochim. Acta*, 2013, **108**, 666-673.
- 34 Y. A. Kim, K. Fujisawa, H. Muramatsu, T. Hayashi, M. Endo, T. Fujimori, K. Kaneko, M. Terrones, J. Behrends, A. Eckmann, C. Casiraghi, K. S. Novoselov, R. Saito, M. S. Dresselhaus,

ACS Nano, 2012, **6**, 6293-6300.

35 J. Chen, Z. H. Zhu, S. Wang, Q. Ma, V. Rudolph and G. Q. Lu, *Chem. Eng. J.*, 2010, **156**, 404-410.

36 L. Li, X. Wang, X. Zhao and M. Zhao, *Phys. Lett. A*, 2013, **377**, 2628-2632.

37 L. Li and M. Zhao, *Phys. Chem. Chem. Phys.*, 2013, **15**, 16853-16863.

38 H. Liu, J. Gao and J. Zhao, *J. Phys. Chem. C*, 2013, **117**, 10353-10359.

39 X. Zhao, L. Li and M. Zhao, *J. phys.: Condens. matter*, 2014, **26**, 095002.

Tables

<i>Bond</i>	<i>L</i> (Å)			<i>θ</i> (°)	<i>ΔL</i> (%)	
	COF-5	COF5-N ₂	COF5-B ₃		COF-5	COF5-N ₂
C ₁ '-C ₁	1.391	1.366	1.390	120.9	-1.8	-0.1
C ₁ - C ₂ (C ₁ -N)	1.41	(1.404)	1.411	120.8	-0.4	0.1
C ₂ -B (N-B)	1.543	(1.438)	1.545	120.7	-6.8	0.1
B-O	1.404	1.402	1.398	124.4	-0.1	-0.4
O- C ₃ (O-B)	1.383	1.390	(1.405)	105.2	0.5	1.6
C ₃ -C ₄ (B-C ₄)	1.372	1.373	(1.500)	129.1	0.1	9.3
C ₄ - C ₅	1.421	1.423	1.396	118.5	0.1	-1.8
C ₅ - C ₅ '	1.463	1.464	1.476	120.3	0.1	0.9

Table 1 The structural parameters for COF-5, COF5-N₂ and COF5-B₃. The bond lengths (*L*) in COF-5, COF5-N₂ and COF5-B₃. The changes of bond lengths (*ΔL*) in COF5-N₂ and COF-B₃ with respect to the corresponding values in COF-5. The bond angle (*θ*) in COF-5 bond are composed by the two atoms in the bond column and their next atom with an order of C₁', C₁, C₂, B, O, C₃, C₄, C₅ to C₅'.

Figure captions

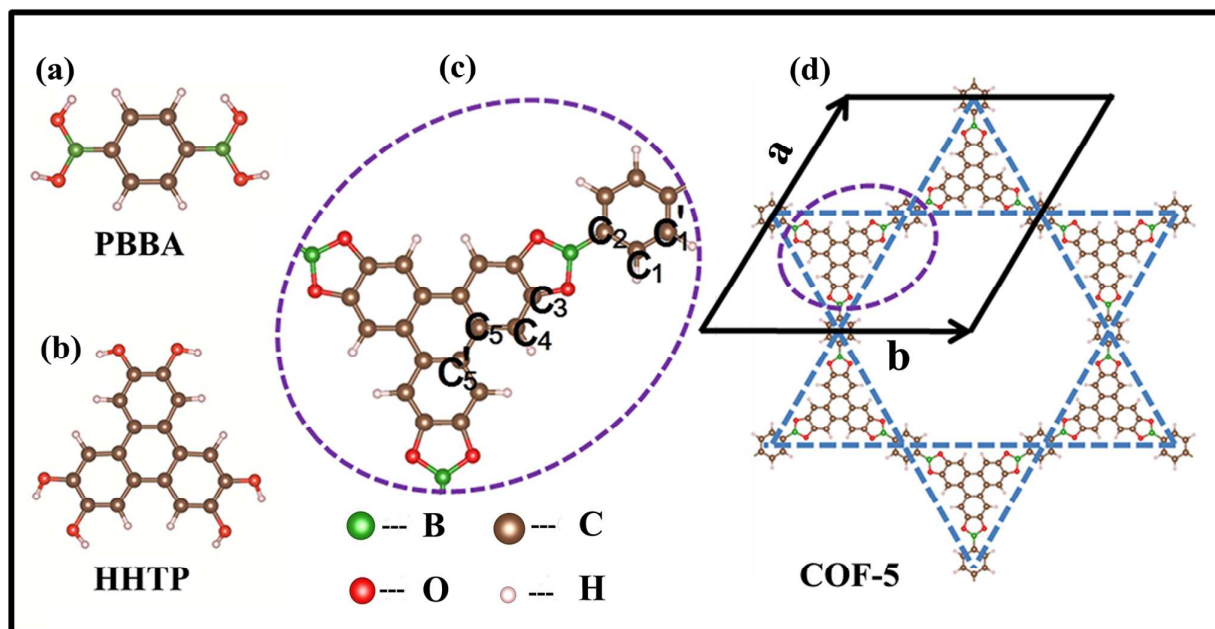


Fig.1 Schematic representation of (a) PBBA, (b) HHTP and (d) the kagome lattice of COF-5. The two basis vectors are represented by \mathbf{a}_1 and \mathbf{a}_2 . (c) The zoom-in map of part in (d) which is circled by dotted line. There are five non-equal atoms for COF-5 donates as C_i ($i=1, 2, 3, 4, 5$). The atoms nearest to the C_1 and C_5 are donates as C_1' and C_5' respectively.

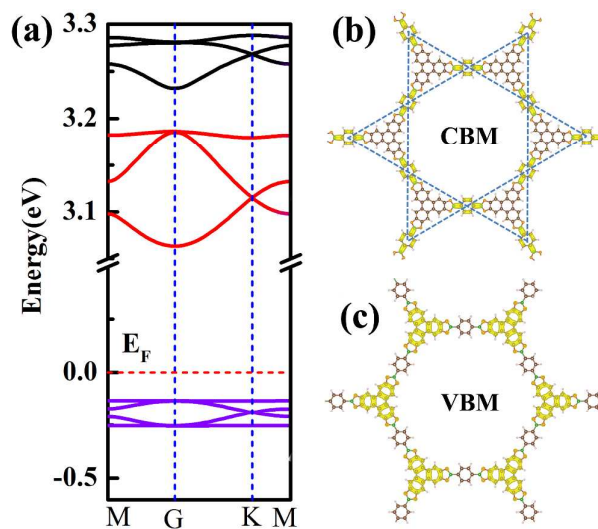


Fig.2 (a) Band lines of COF-5 in proximity of the Fermi level (set to zero) along the high symmetric points in the BZ. M ($1/2, 0, 0$), G ($0, 0, 0$) and K ($2/3, 1/3, 0$) represent the high symmetric points in

the reciprocal space. The typical kagome bands and ruby bands are indicated in red and purple respectively. Charge density isosurfaces of the kagome bands (CBM) and the ruby bands (VBM) nearest to the Fermi level with the isovalue of $0.005 \text{ e}/\text{\AA}^3$ are plotted in (b) and (c).

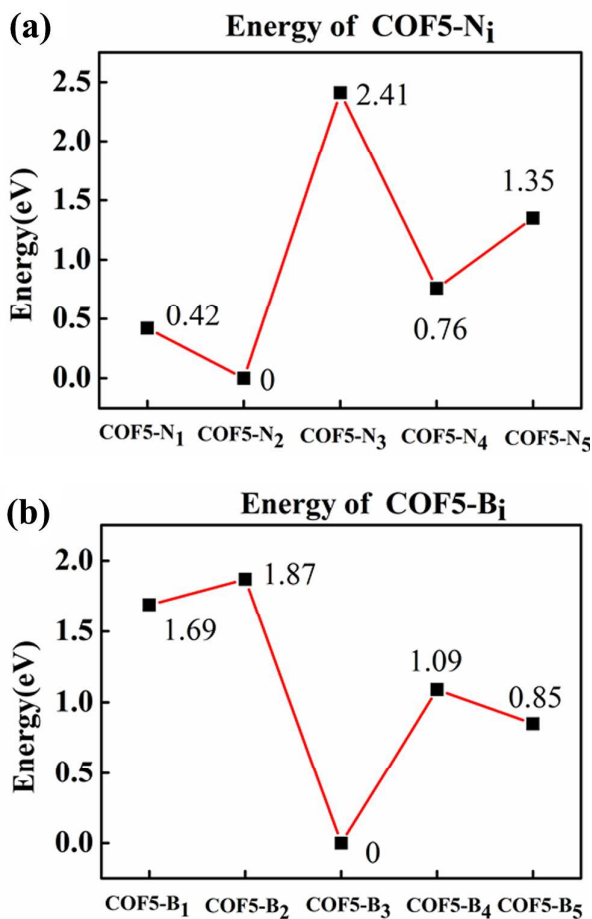


Fig.3 The relative energies for (a) COF5-N_i and (b) COF5-B_i. The energies of the energetically most favorable structures are set to zero.

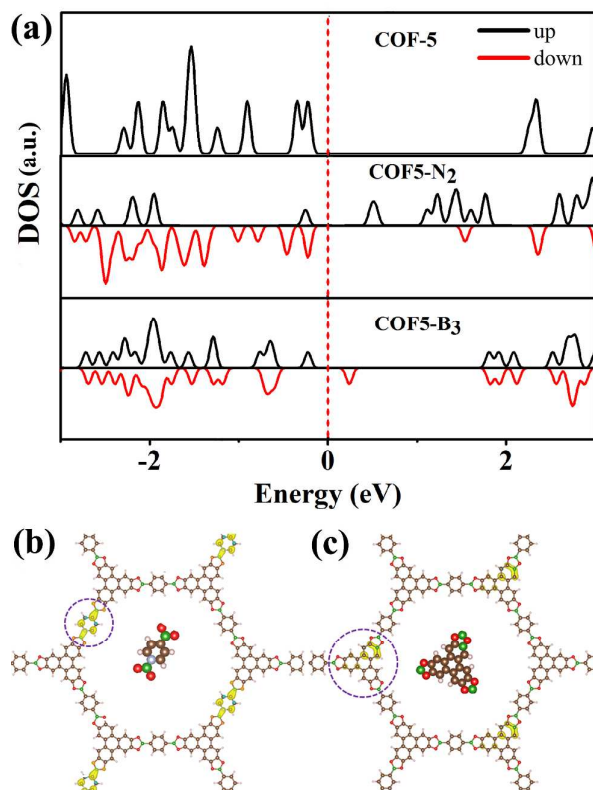


Fig.4 (a) The electron density of states (DOS) of COF-5, COF5-N₂, and COF5-B₃. The spin-polarized charge density ($\rho_{\uparrow}-\rho_{\downarrow}$) for (b) COF5-N₂, and (c) COF5-B₃. The energy at the Fermi level is set to zero. The values of the isosurfaces are set to 0.003 e/Å³. The inset for each part is the zoom-in map of the doping region indicated by the purple circle.

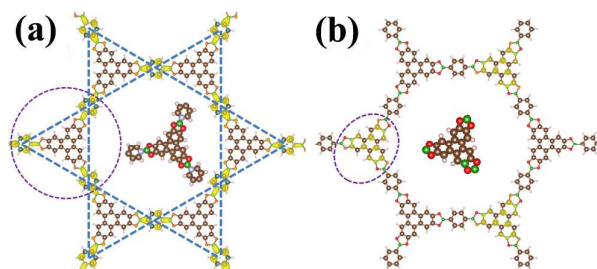


Fig.5 The spin-polarized charge density of (a) COF5-3N₂ and (b) COF5-3B₃ with an absolute isosurface value of 0.003 e/Å³. The inset is the enlarged view of the circle part.

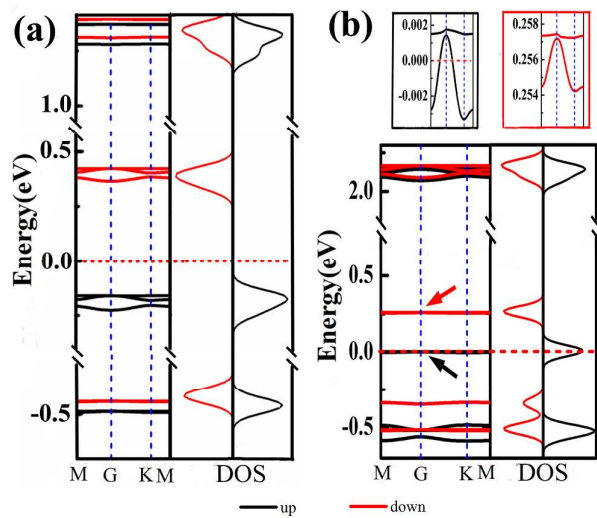


Fig.6 Electronic band structures and electron density of states for (a) COF5-3N₂ and (b) COF5-3B₃. The energy at the Fermi level is set to zero. The up panels of figure (b) are the enlarged views of the flat bands indicated by the arrows.